water

MDPI

Article

Experimental and Numerical Study of Bottom Rack Occlusion by Flow with Gravel-Sized Sediment. Application to Ephemeral Streams in Semi-Arid Regions

Luis G. Castillo *, Juan T. García † and José M. Carrillo †

Hidr@m Group, Department of Civil Engineering, Universidad Politécnica de Cartagena, Paseo Alfonso XIII, 52, 30203 Cartagena, Spain; juan.gbermejo@upct.es (J.T.G.); jose.carrillo@upct.es (J.M.C.)

* Correspondence: luis.castillo@upct.es; Tel.: +34-968-327-012; Fax: +34-968-325-435

† These authors contributed equally to this work.

Academic Editor: Y. Jun Xu

Received: 2 February 2016; Accepted: 14 April 2016; Published: 21 April 2016

Abstract: Rainfall runoff collection in ephemeral streams is an objective in semi-arid zones. Rack intake systems are proposed to collect these flash floods with intensive sediment transport. The design parameters address the problem of clogging the spacing between bars. Experiments for two different void ratio racks are shown. Flows, longitudinal slopes in the rack, and water with three gravel-sized sediments were tested. Results such as effective void ratio due to the gravel deposition over the rack, the evolution of the flow rejected during each test, and the quantification of materials collected and deposited, are presented. The optimal longitudinal rack slope seems to be close to 30%. The effective void ratio is related to several hydraulic parameters calculated at the beginning of the rack. Some adjustments were proposed to predict the effective void ratio.

Keywords: semiarid region; bottom intake system; racks; gravels; laboratory measurements; numerical simulation; sediment transport

---

1. Introduction

Bottom rack intakes are used in mountain streams with rapidly changing flow rates, shallow waters with high velocities, and sediment laden transport ranging from sand to boulders. In some cases, there are debris flows that can reach volumetric concentrations of solids between 15%–30% in the presence of mud flows [1,2]. These regions make difficult the building of large dam-reservoir systems. Small dams would be easily filled by sediments. An intake system may be used to avoid the sedimentation problems. Examples can be found in regions such as the French Alps [1,3], the Tyrol for the TIWAG—Tiroler Wasserkraft AG company [4,5], the Caucasus for the Borjomi water company [6], and La Palma Island (Canary Islands, Spain) for the irrigation society of Heredamiento de las Haciendas de Argual y Tazacorte [7] shown in Figure 1.

Figure 1. Bottom rack intake at the riverbed of Las Angustias Gully—Caldera de Taburiente, located in La Palma Island (Canary Islands, Spain).

This paper is focused on the viability of using an intake system to ephemeral rivers in the semi-arid region of the South East of Spain. Specifically the Albujón Gully was studied, whose morphology and hydrology were extensively characterized in recent years [8–12].

To avoid the obstruction of the racks, recommendations are based on prototype observations [1–5]:

- Bar clearance higher than the d_{90} grain size transported during flood events. Recommended spacing between bars is 0.100–0.120 m in general cases (0.020–0.030 m in cases of water power plants).
- Longitudinal rack slope 20%–60% to reduce the probability of sediment deposition over it.
- Increment of the opening area of the rack by consideration of the surface partially clogging with a factor of around 1.5–2.0.
- Construction of an upstream stilling basin that regulates the size of the incoming sediments.

In clear water flows, some experimental studies are available. Analytical solutions can be obtained considering some assumptions: one-dimensional steady spatially varied flow; incompressible flow; frictionless; hydrostatic pressure distribution; energy head E_0 (or the energy level H_0) constant along the rack (Figure 2). The following equations are obtained considering the energy head remaining constant [13]:

$$\frac{dh}{dx} = -\frac{2C_q m\sqrt{h\cos\alpha(E_0 - h\cos\alpha)}}{2E_0 - 3h\cos\alpha} \quad (1)$$

$$\frac{dq}{dx} = -C_q m \sqrt{2gh\cos\alpha} \tag{2}$$

where dx is an incremental length considered in the flow direction, m the void ratio of the rack, C_q the discharge coefficient, h the water depth measured in the vertical direction, g the gravity acceleration, and α the angle between the horizontal and the rack plane.

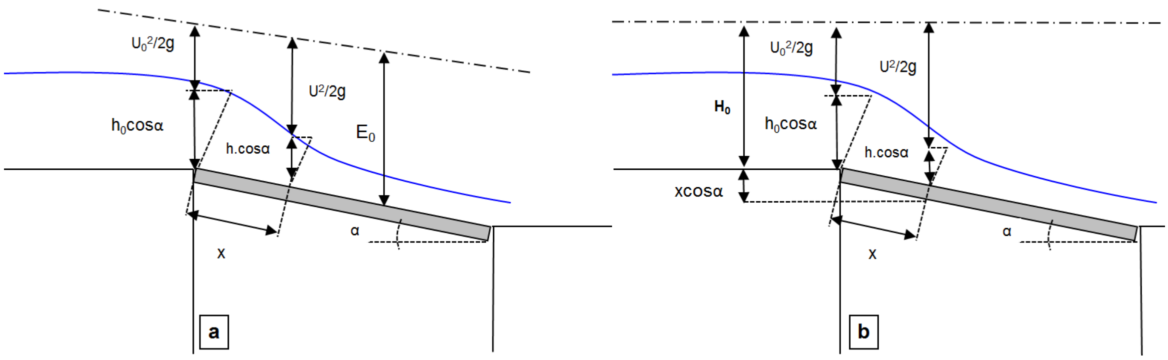

Figure 2. Scheme of longitudinal flow profile over the bottom racks for constant specific energy head (**a**) or constant energy level (**b**).

Several researchers experimentally analyzed these simplifications with clear water flow in hydraulic models. Noseda [14] measured the behavior of racks with T shape bars parallel to the flow direction. The author defined an expression to calculate the discharge coefficient C_q, valid from horizontal to 20% rack slopes and subcritical approximation flows:

$$C_q = 0.66 m^{-0.16} \left(\frac{h}{l}\right)^{-0.13} \tag{3}$$

where l refers to the inter-axis distance between bars.

Righetti and Lanzoni [15] calculated the differential flow collected with a differential equation:

$$dq(x) = C_q m \sqrt{2g(H_0 + x\cos\alpha)}dx \tag{4}$$

The researchers considered that $C_q \approx \sin\theta$, with θ being the angle between the rack plane and the velocity vector.

The differences between the computed water profile with previous Equations (1) and (2), and the values experimentally measured are found in two regions [16]: at the initial part of the rack due to hydrostatic assumption, and at the end of the intake system for the frictionless hypothesis.

Several researchers proposed expressions to calculate the rack length L needed to collect a required flow (Table 1). Noseda [14] considered an analytical integration of Equations (1) and (2). In the same way, Bouvard [17] and Bouvard and Kunztmann [18] supposed the energy level H_0 to be constant. Frank [19,20] calculated the required length of the rack with the hypothesis that the water profile is similar to an ellipse. Krochin [21] included a factor to consider the rack occlusion.

Table 1. Formulations for wetted rack length.

Author	Formulation
Noseda [14]	$L = \frac{E_0}{C_q m}\left[\Phi(y_2) - \Phi(y_1)\right]$; $\Phi = f(y)$; $y = \frac{h}{E}$ $L = 1.1848\frac{E_0}{C_q m}$ $\Phi = \frac{1}{2}\arccos\sqrt{y} - \frac{3}{2}\sqrt{y(1-y)}$ E_0 = specific energy head at the beginning of the rack
Bouvard and Kunztmann [18]	$L = \left\{\frac{1}{2m''}\left[\left(j + \frac{1}{2j^2}\right).\arcsin\sqrt{\frac{j}{j+(1/2j^2)}} + 3\sqrt{\frac{1}{2j}}\right] + \left(\frac{0.303}{m''^2} + \frac{2j^3-3j^2+1}{4j^2}\right)tg\varphi\right\}h_1\cos\varphi$ $j = \frac{h_1}{h_c}$; $m'' = mC_q$ h_1 = flow depth at the beginning of the rack; h_c = critical depth; m'' = product of void ratio and discharge coefficient
Frank [19,20]	$L = 2.561\frac{q_1}{\lambda\sqrt{h_1}}$; $\lambda = mC_{q0}\sqrt{2g\cos\varphi}$; $C_{q0} = 1.22C_{q_{x=x_0}}$ h_1 = flow depth at the beginning of the rack; q_1 = specific approximation flow; α = angle of rack with horizontal
Krochin [21]	$L = \left[\frac{0.313q_1}{(C_q k)^{3/2}}\right]^{2/3}$; $k = (1-f)\,m$; $f = 0.15 - 0.30$ $C_q = C_0 - 0.325tg\alpha$ $C_0 = 0.6$ if $m \geqslant 4$ $C_0 = 0.5$ if $m < 4$ q_1 = specific approximation flow; f = obstruction coefficient

The shape of the bars has also been analyzed to determine the amount of collected flow [1,5,14,19,20,22–24].

Nowadays, a study that focuses on flows with sediment transport is required to verify these design recommendations. Ahmad and Kumar [25] studied in the laboratory the percentage of solids passing through the rack. The authors considered the longitudinal rack slope, different water flows, the ratio between the size of sediments, and the bar clearance (from 0.18 to 0.83). Castillo *et al.* [26–28] carried out numerical simulations with CFD methodology. They analyzed the increment in the wetted rack length due to the sediment transport. Different sediment concentrations, from 1.0% to 5.0% in volume, void ratios from 0.16 to 0.60, flow rates, and rack slopes were all considered.

Taking into account preliminary studies, this work analyses the clogging effects in the rack system. The study is focused on the influence of gravels whose median diameter d_{50}, is close to the spacing between the bars. Those gravels may be trapped by the rack, may block the spacing between bars (reducing the intake surface) or may continue to the downstream side.

2. Experimental Setting

2.1. Physical Device

Tests were carried out in a 5.00 m long, 0.50 m wide and 0.30 m height channel. The channel ends in a bottom rack with variable slope (Figure 3). Flows passing through the rack and rejected are collected by two different channels. The total flow rate that enters in the main channel is measured by an electromagnetic flowmeter. Rejected flow rates are measured by a 90 degree V-notch weir. The racks are formed by T shape bars (T 30/25/2 mm) with a length of 0.90 m and are aligned longitudinally to the principal flow. Three different spacings are adopted which lead to three different racks. Table 2 summarizes the geometric characteristics of each rack.

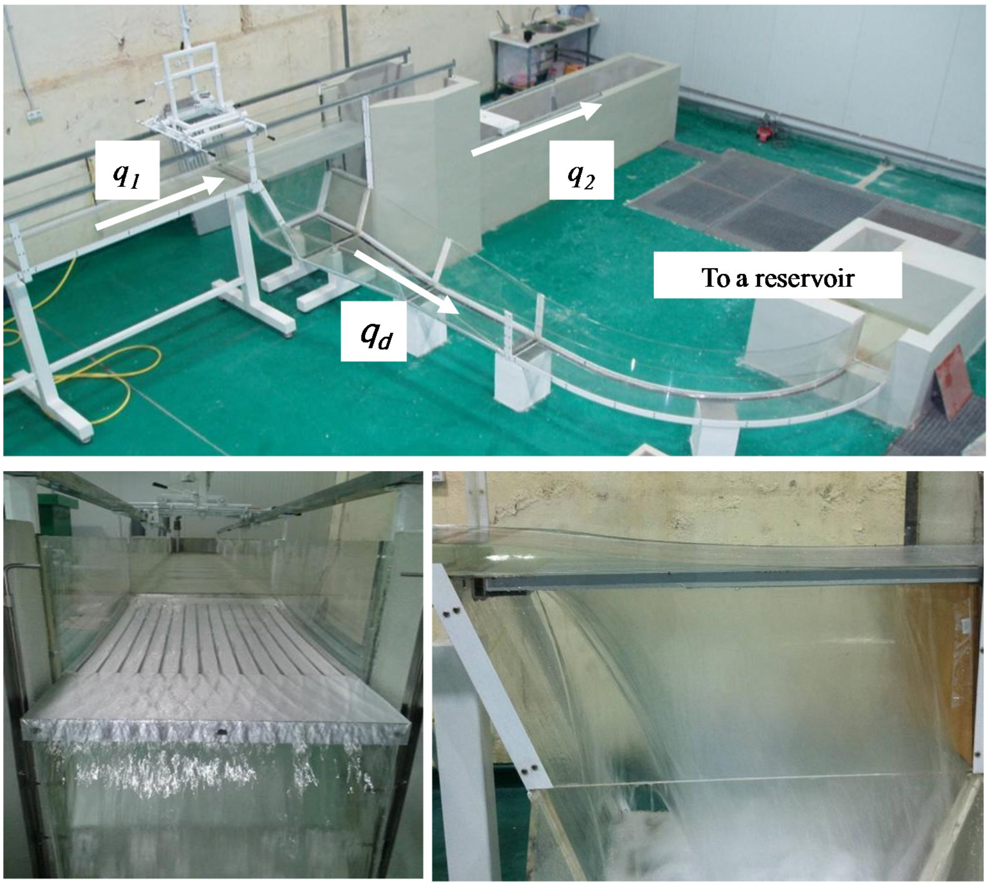

Figure 3. Intake system physical device in the Universidad Politécnica de Cartagena.

Table 2. Geometric characteristic of racks in the physical device.

	A	B	C
Space between bars b_1 (mm)	5.70	8.50	11.70
Void ratio $m = \frac{b_1}{b_1+30}$	0.16	0.22	0.28

2.2. Clear Water Experimental Tests

Specific flows up to 155.4 l/s/m and rack slopes from horizontal to 33% have been considered. Inlet and rejected flows, called q_1 and q_2 respectively, were measured. Flow collected by the rack, q_d, was calculated as a difference between q_1 and q_2. In each test, the height of water was measured by a gage.

Brunella and Hager [16] proposed an expression to calculate the critical Reynolds number in the bottom intake system case. According to the authors, there are no scaling effects when the value is bigger than 250,000. In the tests carried out, the critical Reynolds number was between 287,000 and 678,000. Following [16], no scale effects are expected.

2.3. Numerical Simulations with Clear Water

The clear water hydraulic behavior of the racks were also analyzed with computational fluid dynamics (CFD) programs. The laboratory data were used to estimate the accuracy of the simulations. These codes solve the differential Reynolds-Averaged Navier-Stokes (RANS) equations to satisfy the balance of the governing equations in the three directions. The main equations (mass and momentum conservations) may be written as:

$$\frac{\partial \rho}{\partial t} + \frac{\partial}{\partial x_j}\left(\rho U_j\right) = 0 \quad (5)$$

$$\frac{\partial \rho U_i}{\partial t} + \frac{\partial}{\partial x_j}\left(\rho U_i U_j\right) = -\frac{\partial p}{\partial x_i} + \frac{\partial}{\partial x_j}\left(2\mu S_{ij} - \rho\overline{u_i' u_j'}\right) \quad (6)$$

where x_i defines the coordinate directions (i = 1 to 3 for x, y, z directions, respectively), t the time, ρ the flow density, p the pressure, U the velocity vector, $u_i{}'$ the turbulent velocity, S_{ij} the mean strain-rate tensor, μ the molecular viscosity, and $-\rho\overline{u_i' u_j'}$ is the Reynolds stress.

The finite volume ANSYS CFX (v 14.0) program was used [29]. Following previous studies [26–28], the k-ω based Shear-tress-Transport (SST) model was used to solve the closure problem of the Reynolds averaged Navier-Stokes equations (RANS). The homogeneous model was selected to solve the air-water flow. This model can be viewed as a limiting case of Eulerian-Eulerian multiphase flow in which the interphase transfer rate is very large. This results in all fluids sharing a common flow field, as well as other relevant fields such as turbulence [29]. Around 350,000 elements were used in the simulations. The mesh size near the rack was 0.004 m.

The fluid domain consists of three bars that form two spacings. Symmetry conditions were considered in the vertical planes delimitated by the extreme bars.

The boundary conditions of the simulation are the flow at the inlet, the water depths, and the hydrostatic pressure distributions. For the channel which receives the water passing through the rack plane, an opening boundary condition was used. This condition allows the fluid to cross the boundary surface in either direction. In this study, the free surface is considered as an iso-surface on the 0.5 air volume fraction. Figure 4 shows the velocity vectors in rack C, with 30% slope and q_1 = 138.88 l/s/m.

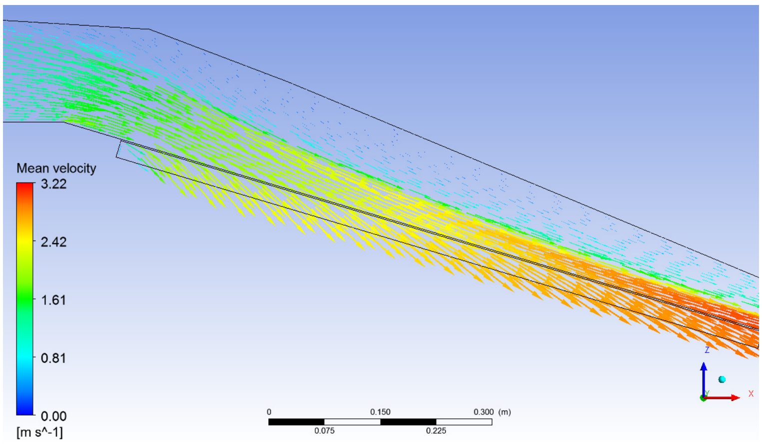

Figure 4. Velocity vectors calculated with numerical simulations for rack *C* (m = 0.28), q_1 = 138.88 l/s/m and 30% slope.

2.4. Sediment Experimental Tests

Occlusion phenomena of bottom racks were evaluated through three gravel-sized materials. The sieve curves are almost uniform. The median grain size is d_{50} = 8.30 mm for gravel 1, d_{50} = 14.80 mm for gravel 2, and d_{50} = 22.00 mm for gravel 3. Gravels 1 and 3 are rounded and gravel 2 is a fracture faces material.

Racks with void ratio m = 0.22 and m = 0.28, called *B* and *C* respectively, were used to test the gravel transport. Gravel 1 was tested with rack of void fraction m = 0.22, using three specific flows (q_1 = 77.0, 114.6, and 155.4 l/s/m), and five slopes (i = 0, 10%, 20%, 30%, and 33%). Gravel 2 and gravel 3 were tested with a rack of void fraction m = 0.28, three specific flows (q_1 = 114.6, 138.88

and 155.4 l/s/m), and the same five slopes. Each condition was repeated once. That made a total of 90 gravel tests.

One hundred kilograms of gravel was dosed at the inlet channel. The solid flow at the beginning of the channel was q_s = 0.33 kg/s. Considering the water flow tested, solid concentrations in volume at the inlet of the channel were between 0.16% and 0.34%. Tests were continued until all solids reached the downstream side of the rack. The duration of the test was between 700 and 1620 seconds.

3. Results and Discussion

3.1. Clear Water Tests

3.1.1. Longitudinal Flow Profile

The longitudinal flow profiles over the center of the bars calculated with CFD were compared with the experimental water depth measurements in the laboratory. Differences around one millimeter indicate a good agreement between the numerical and experimental values. In Figure 5, the longitudinal flow profiles are shown for different specific flows in case of void fraction m = 0.28. From the five racks slope tested, the results of the horizontal and 20% slopes are shown. Results allow confirmation of the accuracy of the numerical simulations.

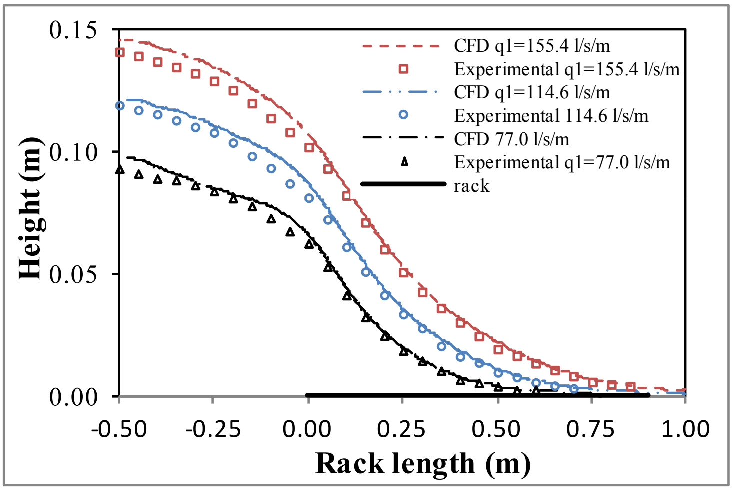

(**a**)

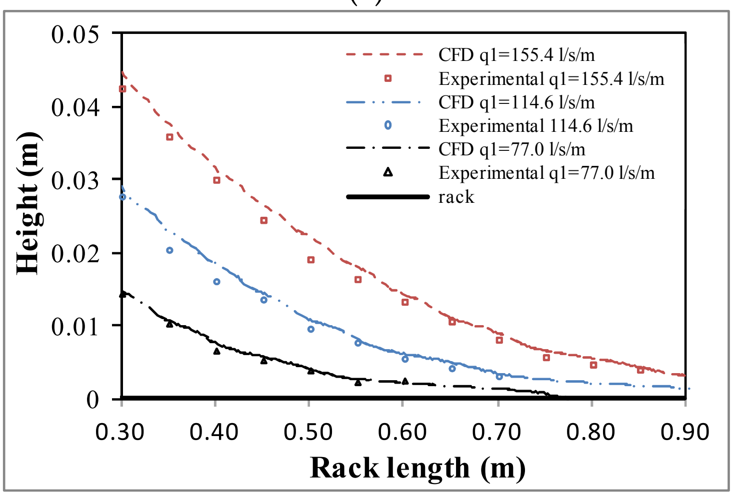

(**b**)

Figure 5. *Cont.*

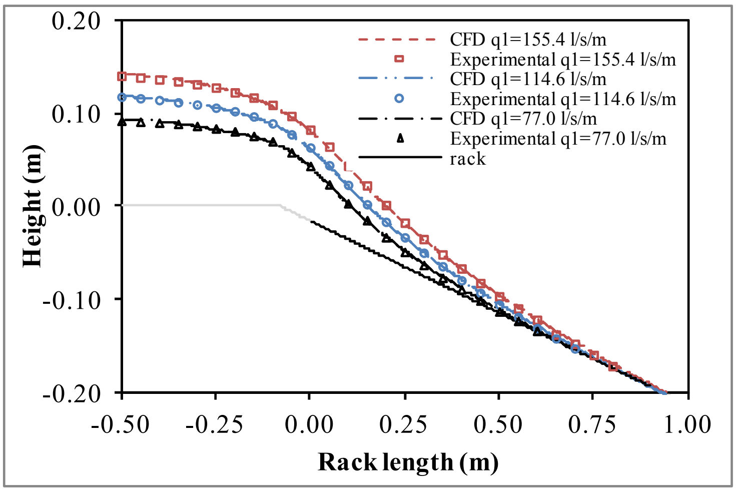

(**c**)

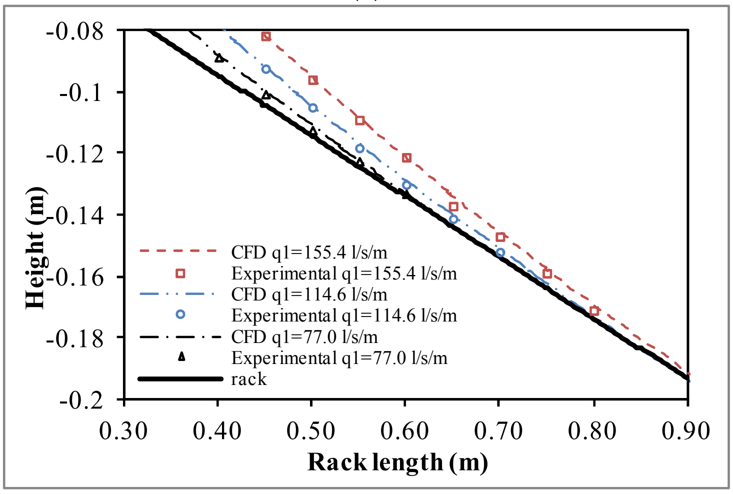

(**d**)

Figure 5. Flow profiles over a bar measured and simulated with computational fluid dynamics (CFD), for horizontal and 20% slope cases, with q_1 = 77.0, 114.6 and 155.4 l/s/m, in the rack *C* (m = 0.28). (**a**,**b**) Rack with slope of 0% ; (**c**,**d**) Rack with slope of 20%.

3.1.2. Discharge Coefficient

Once the numerical models have been calibrated, the inclination of the velocity vector with the plane of the rack is simulated with CFD in the center of the spacing between the bars.

Righetti *et al.* [30] in their lab studies obtained the range of this angle to be between 25 and 35 degrees, for the horizontal slope cases, reducing according to water depth decreases. The sinus of this angle may be used to estimate the discharge coefficient of the water collected through the rack referring to the energy depth [15].

Although the model is not the same as that used by [30], the values obtained with CFD are in agreement with those observed in their experiments, reducing the angle with decreasing water depth over the rack. Figure 6 shows the results of numerical simulations obtained for the specific flow q_1 = 155.4 l/s/m and for rack *C* (m = 0.28), adopting different slopes. The angle of the velocity vector tends to increase with the slope of the rack, referring to the horizontal.

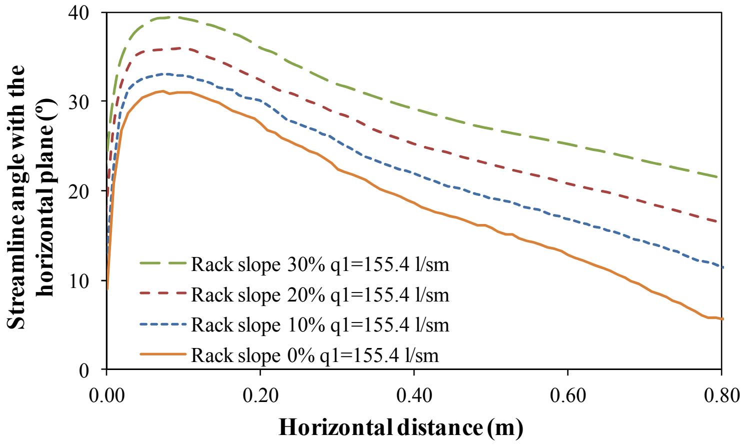

Figure 6. Angle of the velocity vector with the plane of rack *C* for q_1 = 155.4 l/s/m and different longitudinal rack slopes.

3.2. Sediment Tests

3.2.1. Deposition over the Racks

In the experiments, part of the gravel is deposited over the spaces between the bars. This effect generates an increment in the height of the water (Figure 7). This confirms a reduction of the void fraction resulting in an increment of the rejected flow.

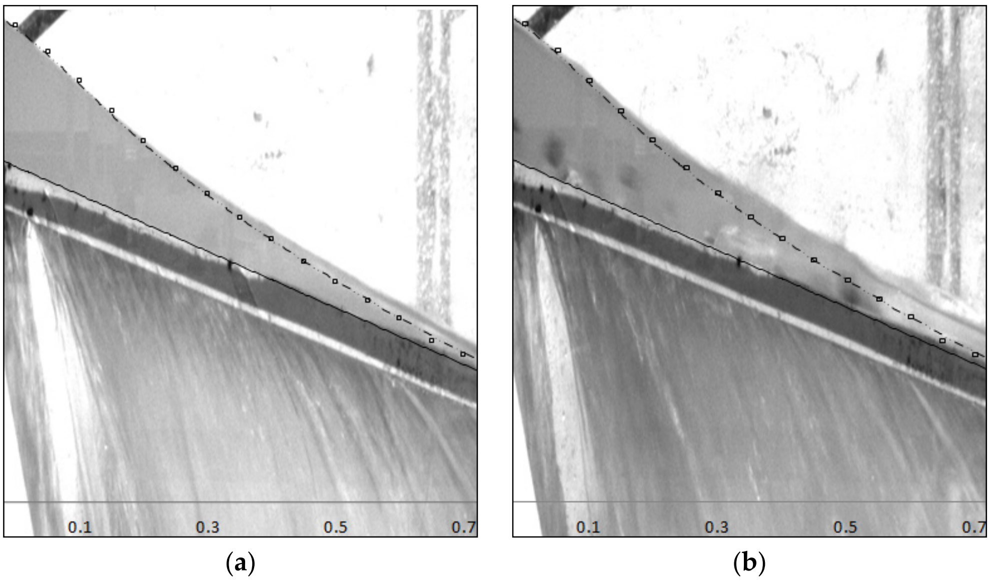

Figure 7. Water profiles over the rack for rack *C* (m = 0.28), 20% slope and q_1 = 155.4 l/s/m. (**a**) Clear water case; (**b**) Water with gravel 2 case.

Flow rejected, q_2, increases during each experiment. Figure 8 shows the variation of rejected flow according to gravel deposition along the test for the case of gravel 1 and gravel 2 with the inlet flow of q_1 = 114.6 l/s/m. The higher increments of rejected flow occur at the beginning of the tests, followed by a stabilization of the collected flow. At the end of the experiments, the rejected flow seems to reach a constant value. The results show a preferential deposition zone. Once it is occluded, no more gravel is deposited over the rack.

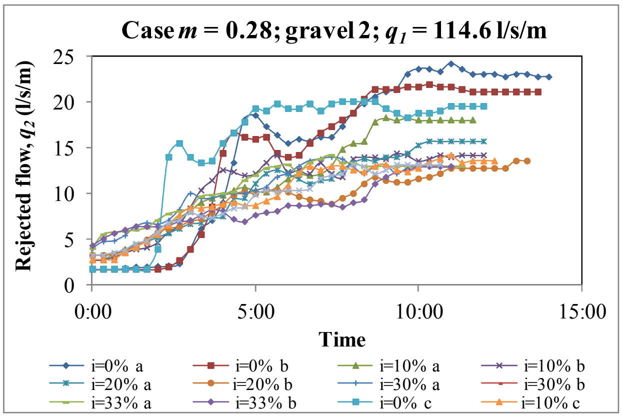

(**a**)

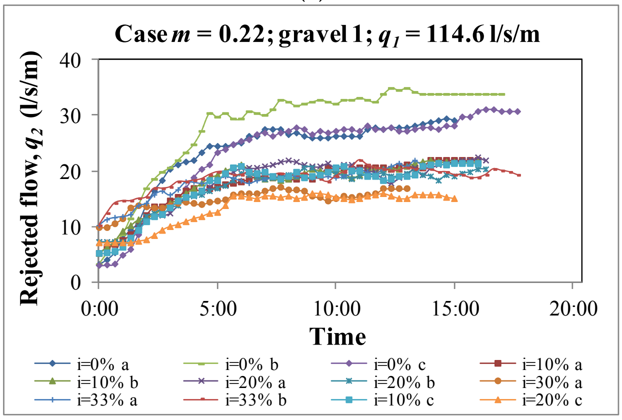

(**b**)

Figure 8. Time evolution of the rejected flow for different longitudinal rack slopes and test with q_1 = 114.6 l/s/m and two different void fractions (m = 0.22 (**a**) and 0.28 (**b**)).

In general, a lower rack slope with gravel transport drives to higher rejected flow, q_2. This is opposed to the clear water case, where the smaller slopes result in lower values of rejected flow. It should be highlighted that differences are observed between the rejected flow in horizontal racks and the other slopes, due to the large obstructions reached with the horizontal slope.

The deposition produces a retention effect that can lead to a complete occlusion if the gravel is not swept. This case is also reflected from a bottom rack in the French Alps [1]. In laboratory experiments, this situation is shown in Figure 9, where the rejected flow reaches minimum values due to the accumulation of gravels at the end of the rack.

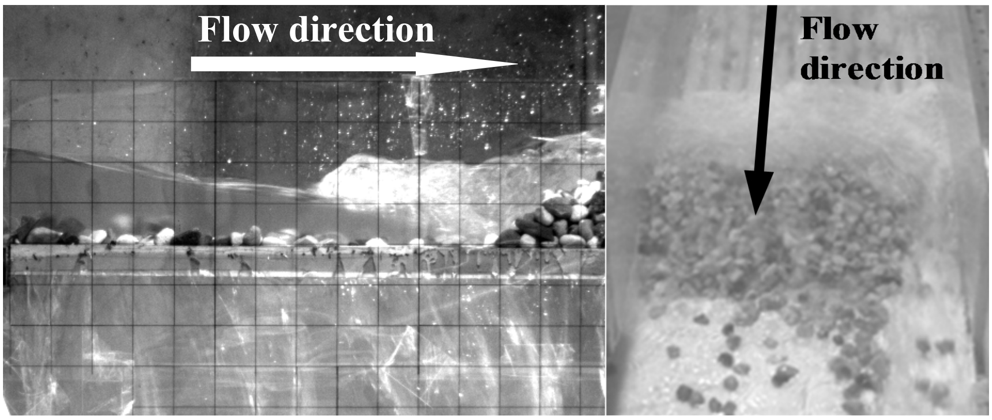

Figure 9. Deposition of gravels over the rack for the horizontal rack slope, rack C, gravel 3 and q_1 = 114.6 l/s/m test.

3.2.2. Efficiency of the Rack

At the end of each sediment test, the ratio between the collected and the inlet flow, $(q_1-q_2)/q_1$, is compared with the clear water situation (Figure 10) in case of rack B (m = 0.22) and q_1 = 77.0; 114.6; 155.4 l/s/m. The longitudinal slope of 30% is the most efficient situation when the occlusion due to gravels is considered in all tests.

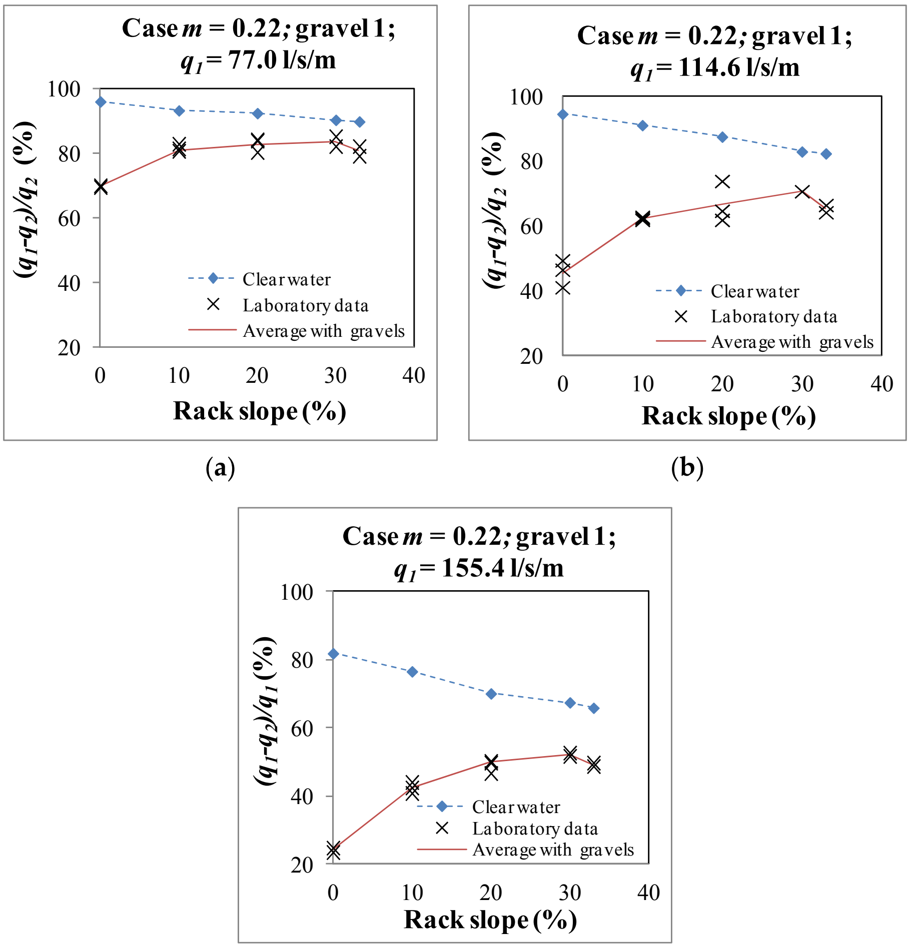

(c)

Figure 10. Percentage of material collected by the rack for diverse tests (**a**) q_1 = 77.0 l/s/m, (**b**) q_1 = 114.6 l/s/m, (**c**) q_1 = 155.4 l/s/m.

3.2.3. Effective Void Fraction

Figure 11 shows the deposition/obstruction zones along the rack for rack C, q_1 = 114.6 l/s/m and horizontal and 30% slopes. At the beginning of the rack there is a non-deposition area due to the initial fall distance of gravel. This distance tends to increase with the rack slope, and the size and weight of the gravels. Later, there is a preferential deposition area, followed by an area where there is no deposition. At the end of the rack, there is a stagnation zone because the spacing between bars disappears.

Deposition of gravel over the bars occurs in areas where the angle of velocity vector with the rack plane is higher. This is in agreement with other researches in this field [15,31–34].

The occluded lengths of the space between bars are measured, and a void ratio can be quantified as shown in Figure 11. Solving Equations (1) and (2) with the discharge coefficient C_q proposed in

Equation (3), and considering the new measured void ratio, a value of the rejected flow smaller than that measured in the lab is obtained.

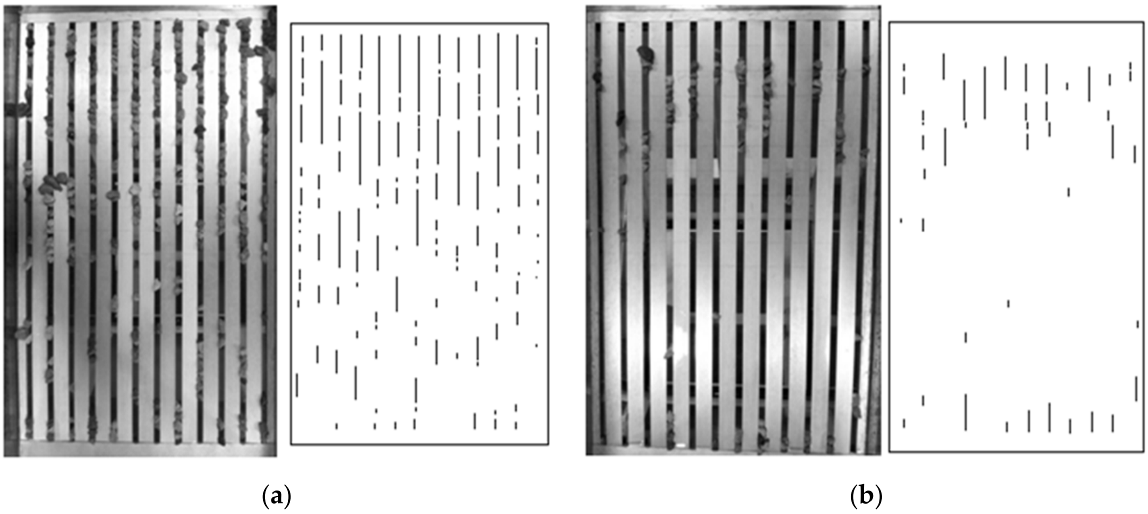

Figure 11. View of racks occlusion at the end of tests for q_1 = 114.6 l/s/m: (**a**) Rack *C* and horizontal slope; (**b**) Rack *C* and 30% slope.

To define the effective void ratio in the occluded racks, m', the differential equation of constant energy head, obtained introducing Equations (2) and (3) into Equation (1), is numerically solved using the fourth-order Runge–Kutta algorithm. It results in a trial and error process varying the value of the effective void ratio m' until the rejected flow measured in the laboratory is reached. The system of equations is equivalent to the solution of two ordinary differential equations for $h(x)$ and $q(x)$. At the inlet section, boundary conditions considered are: the inlet specific flow q_1 and the initial energy E_0 (estimated as the critical energy head), and flow depth at the beginning of the rack, h_0. The numerical computation interval for x is 0.05 m and for the rack length of 0.90 m.

Figure 12 shows the effective void ratios, m', in case of rack *C* (m = 0.28) and gravel 2. As expected, the decrease in void ratio from their values with clear water is more important when there are smaller rack slopes and reduced approximation flows.

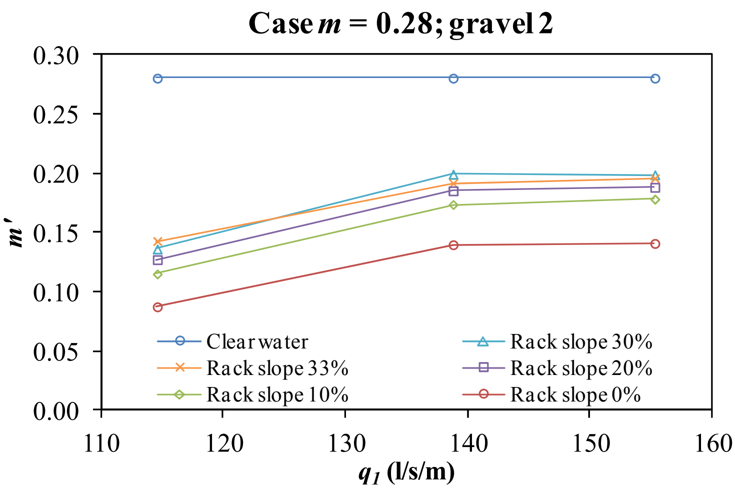

Figure 12. Effective void ratio values m', in case of rack *C* (m = 0.28) and gravel 2.

3.2.4. Effective Wetted Rack Length

From these effective void ratios, m', Equations (1)–(3) have been re-evaluated to calculate the total wetted rack length necessary to collect the total inflow q_1. Figure 13 shows the wetted rack length calculated for gravel 1 and rack *B* (m = 0.22). Data are compared with the wetted lengths calculated by several authors [14,18–21] in the horizontal rack case (see Table 1). Krochin values consider an obstruction percentage f = 30%. The results obtained by Krochin are closer to the laboratory results than those obtained with the formulas proposed by the other authors. Wetted rack lengths with effective void ratios are longer than those measured with clear water. This is due to the gravel occlusion of the bar clearance.

The Noseda's formula is valid in clear water and horizontal racks. If we use this formula to estimate the rack length, 0.93 m are required with rack *B* (m = 0.22) and specific flow rate q_1 = 114.6 l/s/m. When gravel occlusion is considered, this length increases from 1.15 with 30% slope to 1.55 m with horizontal slope.

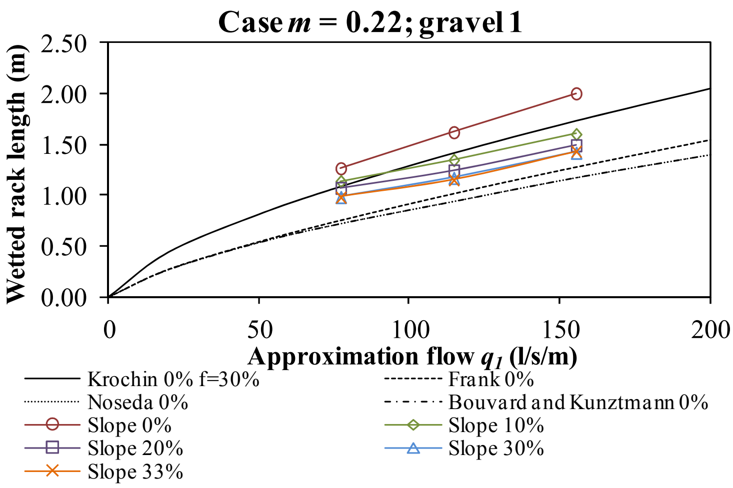

Figure 13. Wetted rack length of rack *B* calculated for each inlet flow rate, different rack slopes and gravel 1.

3.2.5. Relation between Occlusion and Hydraulic Parameters

In Figure 14, the module of the velocity vector U_0 calculated at the beginning of the rack shows a certain lineal tendency with the ratio m'/m.

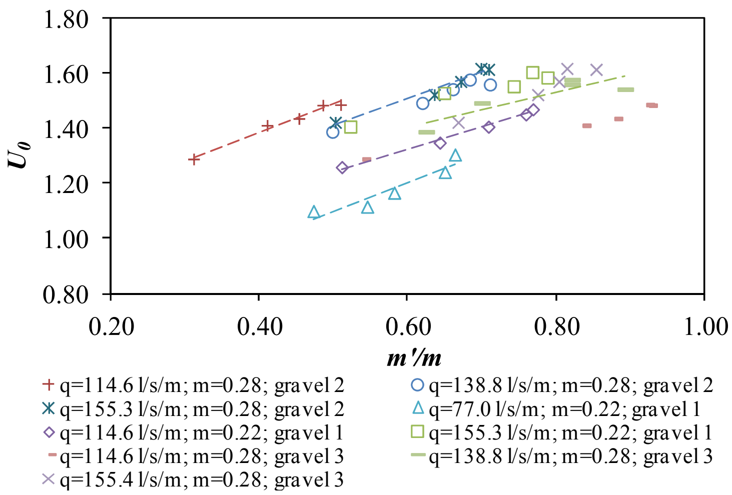

Figure 14. Velocity at the beginning of the rack U_0 as a function of the ratio between the effective and the initial void ratio, m'/m.

Considering the influence of the ratio between the median diameter for the minor axe of the gravel sieve curve and the spacing between bars (d_{50c}/b_1), and the weight of the particles W, an adjustment can be obtained with a correlation of 71%. In this way, Figure 15 shows an adjustment of the hydraulic parameters measured at the beginning of the rack as a function of the m'/m ratio, in which the gravel morphology characteristics are considered:

$$U_0\left(\frac{d_{50c}}{b_1}\right)\left(\frac{1}{W^{0.205}}\right) = 3.0684\left(\frac{m'}{m}\right) + 2.4094 \tag{7}$$

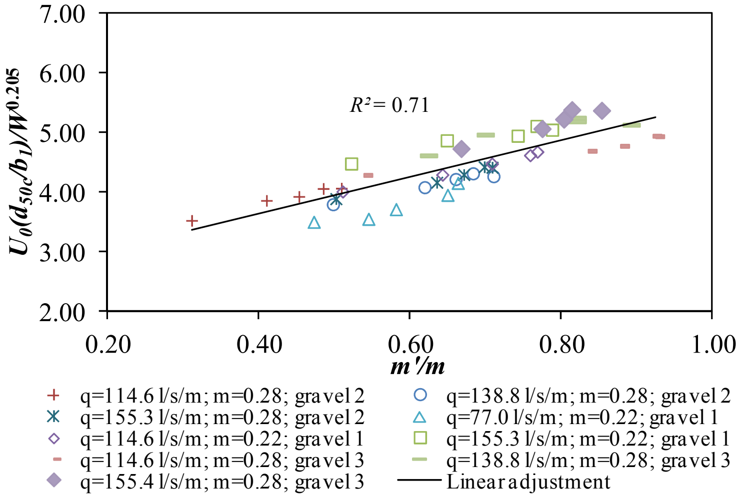

Figure 15. Linear adjustment of the ratio m'/m ratio as a function of the values U_0, d_{50c}/b_1 and W.

Figure 16 compares the values measured in the laboratory with those calculated with the adjustment proposed by Equation (7). The maximum deviations are smaller than 30%.

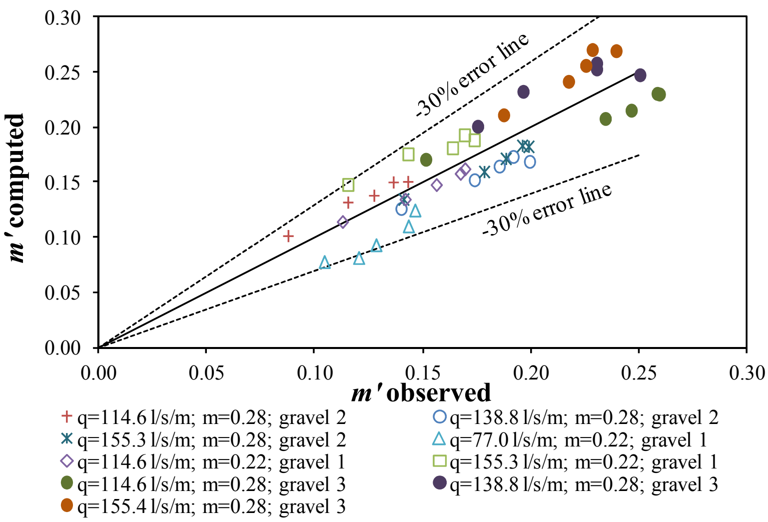

Figure 16. Comparison of observed void ratio with the value computed with Equation (7).

It is remarkable that the adjustment proposed requires an accurate definition of the module of the velocity vector at the beginning of the rack. In Figure 17 an adjustment for the laboratory measures is obtained to calculate the flow depth at the beginning of the rack. Later, the U_0 value can be calculated. The flow depth at the beginning of the rack with a correlation of 87% can be obtained with:

$$\frac{h_0}{h_c} = 5.3072\,(q\cdot i)^{1.4} - 1.552\,(q\cdot i)^{0.7} + 0.8182 \tag{8}$$

where h_0 is the water depth, h_c the critical water depth, q_1 the specific flow, and i the rack slope. The voids of the rack at the physical device start 0.085 m downstream of the inclined plane. For this reason, the ratio h_0/h_c shows values smaller than 0.715 [34,35].

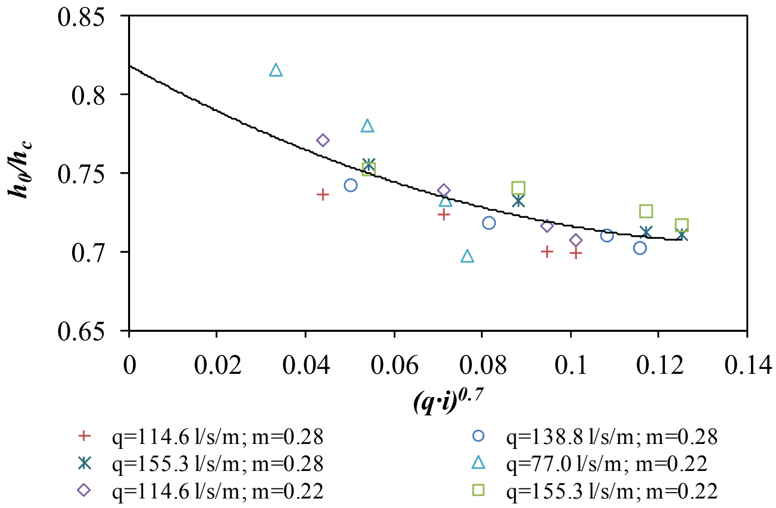

Figure 17. Adjustment of $(q \cdot i)$ with (h_0/h_c).

Equation (7) was used to calculate the effective void ratio. Then, the wetted rack lengths were obtained taking into account the occlusion effect due to gravel-sized materials over the racks. Figure 18 shows the case of rack B (m = 0.22) and gravel 1. In the clear water case, the decrease in the approximation flow rate q_1, results in a reduction of the wetted rack length. In tests with gravels, designers also need to consider the decrease in the effective void ratio, which tends to increase the wetted rack length. The prevalence of one of these opposite effects justifies the observed peaks in the figure.

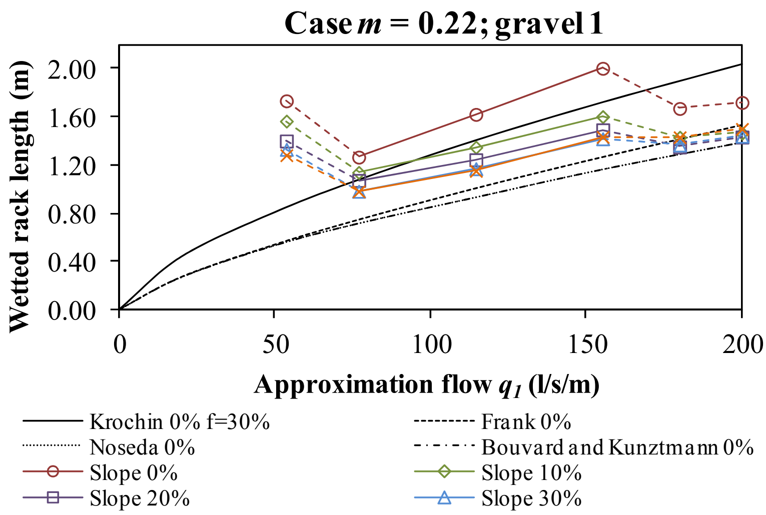

Figure 18. Wetted rack lengths for racks B and gravel 1 defined with experimental test and adjusted (dashed line) with Equation (7).

4. Conclusions

Bottom intake systems were analyzed in order to utilize them in ephemeral rivers of semi-arid regions, such as in the South East of Spain (Albujon Gully). In these areas, the rain episodes generate flood events with intense sediment transport. The objective of these structures is to collect water avoiding the rack obstruction. The shape of bars and spacing between them, as well as the longitudinal rack slope are parameters that need to be considered as a function of the sediment transport that occurs in the river. Design criteria of bottom rack intake systems in mountain rivers usually consider a bar clearance higher than d_{90}. This study enables the behavior to be known of bottom rack intake systems with a reduced bar clearance from the point of view of the occlusion caused by gravel-sized materials.

Around 90 different tests with two different racks (void ratios of 0.22 and 0.28), and three different gravels resulted in the definition of the optimal longitudinal rack slope as 30%. All the experiments had a critical Reynolds number bigger than 250,000 [16]. Results are free of scaling effects.

The effective void ratios, and rack lengths are calculated by experimental measurements of flow with gravels, taking into account the occlusion effect. A linear equation relating the module of the velocity at the beginning of the rack, the ratio of the median diameter of the minor axe size and the space between bars, as well as the weight of the particles is proposed in Equation (7). This allows the increment to be calculated of the wetted rack length in gravels with d_{50} near to or bigger than the spacing between bars. In general, wetted rack lengths considering occlusion are in agreement with the formula proposed by Krochin [21] when an obstruction coefficient of 30% is considered.

Numerical simulations with CFD code obtain results close to those experimentally measured, even with different flows and slopes. This enables the experimental works to be supported, specifically for obtaining the angle of the velocity vector with the plane of the rack between bars, and to calculate the friction angle between gravels and the rack starting from the experimental observations of preferential deposition areas over the racks.

To extrapolate the results to diverse semiarid regions, more experimental studies should be done considering their specific sieve curves, testing racks with different void ratios, slopes, and shape of bars. The methodology proposed can be used to find out the occlusion percentage. In each specific case, the liquid and solid flows that reach the intake system should be defined by field studies.

Acknowledgments: The authors are grateful for the financial support received from the Seneca Foundation of Región de Murcia (Spain) through the project "Optimización de los sistemas de captación de fondo para zonas semiáridas y caudales con alto contenido de sedimentos. Definición de los parámetros de diseño". Reference: 19490/PI/14.

Author Contributions: L.G. Castillo carried out the direction, analysis and planning of laboratory tests and numerical simulations, analyzed the results and participated in written works. J.T. García carried out all test campaigns in the laboratory and participated in written works and J.M. Carrillo carried out the numerical simulation and participated in written works. All authors reviewed and contributed to the final manuscript.

Conflicts of Interest: The authors declare no conflict of interest.

References

1. Bouvard, M. *Mobile Barrages & Intakes on Sediment Transporting Rivers*; International Association of Hydraulic Engineering and Research (IAHR) Monograph: Rotterdam, The Netherlands, 1992.
2. Raudkivi, A.J. *Hydraulic Structures Design Manual*; International Association of Hydraulic Engineering and Research (IAHR): Rotterdam, The Netherlands, 1993; pp. 92–105.
3. Ract-Madoux, M.; Bouvard, M.; Molbert, J.; Zumstein, J. Quelques réalisations récentes de prises en-dessous à haute altitude en Savoie. *La Houille Blanche* **1955**, *6*, 852–878. [CrossRef]
4. Simmler, H. *Konstruktiver Wasserbau, Technische Universität Graz*; Institut für Wasserwirtschaft und konstruktiven Wasserbau: Graz, Austria, 1978.
5. Drobir, H. Entwurf von Wasserfassungen im Hochgebirge. *Österr. Wasserwirtschaft* **1981**, *33*, 243–253.
6. Mostkow, M. Sur le calcul des grilles de prise d'eau. *La Houille Blanche* **1957**, *4*, 569–576. [CrossRef]
7. Castillo, L.G.; Lima, P. Análisis del dimensionamiento de la longitud de reja en una captación de fondo. In Proceedings of the XXIV Congreso Latinoamericano de Hidráulica, Punta del Este, Uruguay, 21–25 November 2010.
8. Conesa, C. *La Acción Erosiva de las Aguas Superficiales en el Campo de Cartagena*; Universidad de Murcia, Departamento de Geografía Física, humana y Análisis Regional: Murcia, Spain, 1989.

9. Conesa, C. *El Campo de Cartagena. Clima e Hidrología de un Medio Semiárido*; Universidad de Murcia, Ayuntamiento de Cartagena, Comunidad de Regantes del Campo de Cartagena: Murcia, Spain, 1990.
10. Navarro, F. *El sistema Hidrográfico del Guadalentín*; Consejería de Política Territorial, Obras Públicas y Medio Ambiente. Cuaderno Técnico No. 6: Murcia, Spain, 1991.
11. Marín, M.D. *Suficiencia Investigadora*; Programa de Doctorado: Minería Medio Ambiente y Desarrollo Sostenible, Grupo I+D+i en Ingeniería Hidráulica y Medio Ambiente HIDR@M: Cartagena, Spain, 2011.
12. Castillo, LG.; Marin, M.D. Hydrological and hydraulic characterization in semiarid zones. Analysis of model type, basin size and sediment transport formulae. In Proceedings of the International Conference on Fluvial Hydraulics, San Jose, Costa Rica, 5–7 September 2012.
13. Garot, F. De Watervang met liggend rooster. *Ing. Ned. Indie* **1939**, *7*, 115–132.
14. Noseda, G. Correnti permanenti con portata progressivamente decrescente, defluenti su griglie di fondo. *L'Energia Elettrica* **1956**, 565–581.
15. Righetti, M.; Lanzoni, S. Experimental study of the flow field over bottom intake racks. *J. Hydraul. Eng.* **2008**, *134*, 15–22. [CrossRef]
16. Brunella, S.; Hager, W.; Minor, H. Hydraulics of bottom rack intake. *J. Hydraul. Eng.* **2003**, *129*, 2–10. [CrossRef]
17. Bouvard, M. Debit d'une grille par en dessous. *La Houille Blanche* **1953**, *2*, 290–291. [CrossRef]
18. Bouvard, M.; Kuntzmann, J. Étude théorique des grilles de prises d'eau du type "En dessous". *La Houille Blanche* **1954**, *5*, 569–574.
19. Frank, J. Hydraulische Untersuchungen für das Tiroler Wehr. *Der Bauing.* **1956**, *31*, 96–101.
20. Frank, J. Fortschritte in der hydraulic des Sohlenrechens. *Der Bauing.* **1959**, *34*, 12–18.
21. Krochin, S. *Diseño hidráulico*, 2nd ed.; Colección Escuela Politécnica Nacional: Quito, Ecuador, 1978.
22. Orth, J.; Chardonnet, E.; Meynardi, G. Étude de grilles pour prises d'eau du type. *La Houille Blanche* **1954**, *3*, 343–351. [CrossRef]
23. White, J.K.; Charlton, J.A.; Ramsay, C.A.W. On the design of bottom intakes for diverting stream flows. In *Proceedings of the Institution of Civil Engineers*; ICE Publishing: London, UK, 1972; Volume 51, pp. 337–345.
24. Drobir, H.; Kienberger, V.; Krouzecky, N. The wetted rack length of the Tyrolean weir. In Proceedings of the 28th IAHR Congress, Graz, Austria, 22–27 August 1999.
25. Ahmad, Z.; Kumar, S. Estimation of trapped sediment load into a trench weir. In Proceedings of the 11th International Symposium on River Sedimentation, University of Stellenbosch, South Africa, 6–9 September 2010; pp. 1–9.
26. Castillo, L.G.; Carrillo, J.M.; García, J.T. Comparison of clear water flow and sediment flow through bottom racks using some lab measurements and CFD methodology. In *WIT Transactions on Ecology and the Environment*; Wessex Institute of Technology: New Forest, UK, 2013; Volume 172, pp. 227–237.
27. Castillo, L.G.; Carrillo, J.M.; García, J.T. Flow and sediment transport through bottom racks. CFD application and verification with experimental measurements. In Proceedings of the 35th IAHR Congress, Chengdu, China, 8–13 September 2013.
28. Castillo, L.G.; Carrillo, J.M.; García, J.T. Comparativa del flujo de agua limpia y con sedimentos a través de sistemas de captación de fondo utilizando datos de laboratorio y un modelo CFD. In Proceedings of the III Jornadas de Ingeniería del Agua, Valencia, Spain, 23–24 October 2013.
29. ANSYS, Inc. *ANSYS CFX-Solver Theory Guide, Release 13.0*; ANSYS, Inc.: Canonsburg, PA, USA, 2010.
30. Righetti, M.; Rigon, R.; Lanzoni, S. Indagine sperimentale del deflusso attraverso una griglia di fondo a barre longitudinali. In Proceedings of the XXVII Convegno di Idraulica e Costruzioni Idrauliche, Genoa, Italy, 12–15 September 2000; Volume 3, pp. 112–119.
31. Castillo, L.G.; Carrillo, J.M. Numerical simulation and validation of intake systems with CFD methodology. In Proceedings of the 2nd IAHR European Congress, Munich, Germany, 27–29 June 2012.
32. Castillo, L.G.; García, J.T.; Carrillo, J.M. Experimental measurements of flow and sediment transport through bottom racks. Influence of graves sizes on the rack. In Proceedings of the International Conference on Fluvial Hydraulics, Lausanne, Switzerland, 3–5 September 2014.
33. Castillo, L.G.; García, J.T.; Carrillo, J.M. Intake systems in ephemeral rivers. In *WIT Transactions on Ecology and the Environment*; Wessex Institute of Technology: New Forest, UK, 2015; Volume 197, pp. 117–128.

34. Montes, S. *Hydraulics of Open Cannel Flow*; American Society of Civil Engineers: Reston, VA, USA, 1998.
35. Rouse, H. *Fluid Hydraulics for Mechanics Engineers*; Dover Publications: New York, NY, USA, 1938.